

AUTOMATED 3D MAPPING OF TREES AND BUILDINGS AND IT'S APPLICATION TO RISK ASSESSMENT OF DOMESTIC SUBSIDENCE IN THE LONDON AREA

Jan-Peter Muller^a, Jung-Rack Kim, Jonathan Kelvin

Dept. of Geomatic Engineering, University College London, Gower Street, London, WC1E 6BT UK
jpmuller@ge.ucl.ac.uk^a

TS ICWG II/IV

KEY WORDS: IKONOS, LIDAR, Vision, DEM/DTM, Urban, Vegetation, GIS, Geology, Subsidence risk assessment

ABSTRACT:

Very high resolution images (e.g. IKONOS) and airborne lidar have been used for the automated 3D mapping of individual tree and building locations in a large test area in East London of some 8 x 8km extent with many tens of thousands of buildings and trees. Initial results of the building and tree detection algorithm for small area assessments were given in Kim & Muller (2002). In this work we report on the extension of the algorithm to the full area and the refinement of the algorithm to extract tree height. Also shown will be the building detection's quantitative assessment using the OS® MasterMap® (Parish et al., 2003, submitted) and the random sample assessment of tree locations using higher resolution digitised aerial photography from different commercial suppliers. Overall the detection efficiency is greater than 75% even though the buildings have a huge range in floorplan, height, age and type. Tree detection efficiency is based on a visual assessment of the degree of overstorey crown overlap but has similarly high values.

1. INTRODUCTION

1.1 Aims

The primary goal of the research work reported here was to develop practical techniques for the automated production of dense landscape object models focussing on buildings and trees in urban area.

With the increasing demands for information on artificial and natural landscape objects in many application fields (e.g. risk insurance, mobile telecommunication, city planning, geological research etc.), newly delivered commercial high-resolution satellite imagery and LiDAR (Light Detection and Ranging) data are stimulating the development of automated GIS construction. This research aims at the retrieval of 3D shape or 2D boundaries of buildings, which are larger than 10 square metres and have some regularity, and individual tree crowns with an acceptable degree of accuracy in very dense urban environments from high-resolution images and range data. Data processing algorithms utilising both range and image data or between image clues are here described to address technical problems associated with the available data sources such as, insufficient data resolution to resolve detailed object structure, a very large search area and irregularity of targets (tree and building)..

1.2 Previous research work

Building detection has been one of the major research topics of the photogrammetric community over the last 20 years. A sample of previous work is provided here relevant to the work at UCL and other centres. Kim and Muller (1999) developed a graph-based building reconstruction algorithm using 2D edge lines extracted from aerial photographs. Roux and McKeown (1994) used multiple aerial photos to construct 3D roof models of buildings. Perceptual grouping and shadow information was used for 3D building reconstruction by Lin and Nevatia (1998). The AMOBE project at ETH Zurich (Henricsson et al, 1996) is one of the first examples of the use of colour information for building extraction. Brenner and Halla(1999) constructed 3D building models from Lidar data and multi-spectral information. Marr and Vosselman (1999) suggested algorithms to extract building structures from invariant moments derived from Lidar.

Recently research has begun to examine the application of high resolution satellite images such as IKONOS for building extraction (see, for example, Fraser et al., 2001).

Individual tree crown detection is a very recent topic in image understanding and remote sensing data analysis. Template matching involving the correlation between a pre-defined model and an image patch is one method proposed for automated tree detection (Pollock 1998). Zang (2001) showed the first promising results using texture analysis in high resolution optical urban images. Gong et al. (2002) used a semi-automated interactive 3D model-based tree interpreter from multi-ocular high-resolution aerial images. Straub (2003) used LiDAR and a top-down low level operator to extract tree crown.

1.3 Data description

Space Imaging's IKONOS, which is the first commercial high-resolution satellite imager of the Earth, has unprecedented clarity and detail (nominal IfoV≤1m). IKONOS products use a general photogrammetric model, based on Rational Polynomial Coefficients (Grodecki 2001) Several relevant articles regarding IKONOS photogrammetric modelling accuracy have recently been published. A comprehensive review of IKONOS image radiometric and photogrammetric quality has been performed by Grodecki and Dial(2001) and Baltsavias et al. (2001) respectively. In particular, Grodecki and Dial(2001) showed that, in the case of GCP controlled stereo images (Precision stereo), the accuracies were within 1 metre horizontally and 2 metres vertically. According to this result, the photogrammetric quality of any IKONOS precision data set should be acceptable for urban area mapping, where landscape objects of a few metres' scale are present.

The test data-set used in our study consisted of an IKONOS Pro geocoded single view data set over East London (11 by 11km), which was pan-sharpened to one metre resolution and contains R-G-NIR bands, using an unidentified technique by the satellite supplier. An initial assessment was performed of the planimetric positioning accuracy through an inter-comparison with kinematic (k-GPS). This showed that the planimetric accuracy appeared to be better than it's technical specification. Lidar data supplied by Infoterra Limited came from an Optech 1020 ALS (Airborne Laser scanner) (<http://www.optech.on.ca/>) which was

used as a 3D range data source. This has an average point density of 1 lidar footprint per 3-4 square metres point density. It was quickly established that the point density of this 3D range data was insufficient for reliable object model construction. Hence an image fusion algorithm was developed to address such problems.

2. ALGORITHMS

The overall processing steps are shown in Figure 1. The overall procedure consists of 3 stages. Firstly, regions of interest (ROIs) are defined in a focusing stage using a normalised DEM, n-DEM (i.e. heights above the “bare earth” terrain) and NDVI (Normalised Difference Vegetation Index). These “ROIs” are then refined using multi spectral information from the co-registered optical images.. Then polygons for buildings and ellipses for tree crown are fitted to the refined ROI boundaries to identify buildings and trees in the “identification” stage.

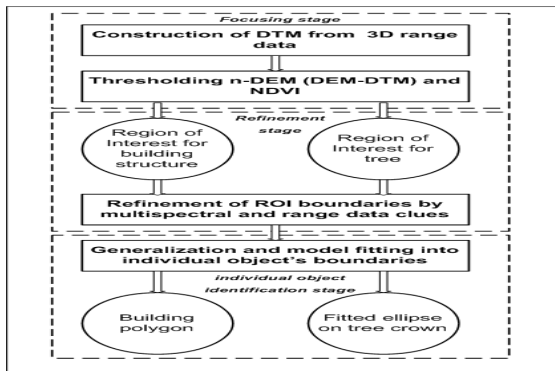


Figure 1. Overall Procedure

2.1 Focusing

A focusing strategy using the n-DEM and multi-spectral information is commonly used. In our case, NDVI for satellite information and normalised colour index from ratios such as (R-G/R+G) originally used for aerial photos, was adopted. A key point in this strategy is the use of 3D range data. There are two common approaches: – a so-called “Top-down” approach, which directly segments the 3D range data and a “Bottom-up” approach (Kraus and Pfeifer 1997, Axelsson 1998, Lohnmann et al. 2000, Vosselman 2000), which attempts to construct a Bare Earth DEM (DTM). The “Bottom-up” approach usually produces a coarser boundary but is more suited to wide area applications due to a lower computational demand. Our “Bottom-up” strategy used a hierarchical scheme to reduce CPU time and update reliability in the reconstructed DTM for dense altitude clusters.

The definition of a seed area is the starting point for Bald Earth construction. 3D range data points are re-binned using (1) to avoid artefacts and the local min-max detection algorithm from Chaudhuri and Shankar (1989) is applied to the newly binned height plane.

$$h_b(n_x, n_y) = \max\left(\sum_{x=1}^{n_x} \sum_{y=1}^{n_y} h(x, y) / h_s\right) \quad (1)$$

where h = height points at x, y coordinates

h_s = vertical renormalized factor

h_b = binned value

$n_x = x/n, n_y = y/n$

n = size of bin, usually at the maximum ALS data resolution

From the detected local min-max points, region growing using the local slope (usually 25°) is used. If the dimensions of the

region-growing sheet is larger than the estimated maximum-building size, it's likely to be a seed area (ground plane). Then two normal distribution are fitted to the height points on the “ground plane” using a window size by Kittler and Illingworth (1986)'s criterion.

$$J(t) = 1 + 2.0(P_1(t) \log \sigma_1(t) + P_2(t) \log \sigma_2(t)) - 2.0(P_1(t) \log P_1(t) + P_2(t) \log p_2(t)) \quad (2)$$

where $P(t)$: the sum of Probability Density Functions (PDFs)
 σ : the standard deviation

Now,

If $\mu_2(t) - \mu_1(t) <$ the estimated object height, then $\mu_1(t)$ is the mean value height of a larger object surface or it is assumed to be a flat ground plane so that the window size then needs to be extended and the estimation repeated.

If $\mu_2(t) - \mu_1(t) >$ the estimated object height, then $\mu_1(t)$ is selected as a seed point within the window.

Using a value of $\mu_1(t)$ and window size, w , a gridding scheme can be applied. The Smith & Wessel (1990) method to interpolate bald earth seed points is employed here. It's one kind of optimisation method for the solution of the following function

$$(1-T) \nabla^2 Z - TVZ = 0 \quad (3)$$

where Z : height points, T : Tension factor between 0.0 to 1.0

When applying this method, a higher tension factor will produce a higher curvature surface. To construct a smoother surface at a lower hierarchical stage, a lower tension factor is required. In the first stage, the lowest tension factor and the largest window size are used to save CPU time.

Figure 2 shows one example of the refinement step in the flat earth surface. As seen in Figure 2, the DTM detail is clearer in the later gridding steps and well preserves flatness.

Now by thresholding the n-DEM (DSM-DTM), the “above surface points which are likely to be either trees and/or buildings” and “surface” points are split. Tree and building areas are simply separated around an NDVI value 0.3. Therefore, “tree ROI” and “building ROI” are defined in this step.

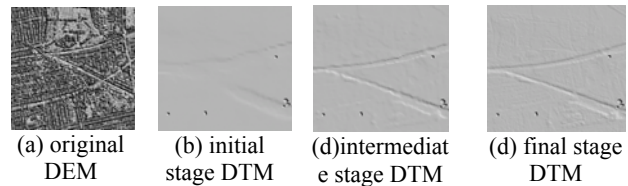


Figure 2. Hierarchical refinement of DTM

2.2 Refinement of region of interest

By labelling isolated areas, a set of ROIs can be defined. However, their boundaries are not sharp because of the poor resolution of the 3D range data (1pixel /3-4 m) compared with optical images.

A strategy to cope with such a situation is the compensation of ROIs through optical image clues using mainly multi-spectral information.

The overall procedure is shown in Figure 3.

The positions of buildings and trees can be identified by locating “above ground” 3D range points. Thus, supervised

classification schemes, where training sets can be found for building and tree height points, can be introduced.

To use 3D range points as training vectors, correct co-registration with optical images is indispensable especially correcting for “building lean effects”. We applied the method proposed by Baltsavias et al.,(2001).

$$\begin{aligned} \Delta X_i &= -\Delta Z \sin(a)/\tan(e) \\ \Delta Y_i &= -\Delta Z \cos(a)/\tan(e) \end{aligned} \quad (4)$$

where ΔZ : normalised height points-Bald earth height angle,
 a : sensor azimuth angle,
 e : sensor elevation angle

This relationship is not very exact but can be used with some margin considering the intrinsic planimetric error of IKONOS Pro image (3-4 metre in here). By combining NDVI and n-DEM heights, training vectors for tree, building and bare earth can be defined. Then a Bayesian supervised classification using individual ROIs can be applied using these training vectors. A Priori probabilities of tree and building areas in a Bayesian classifier can be calculated through (5)

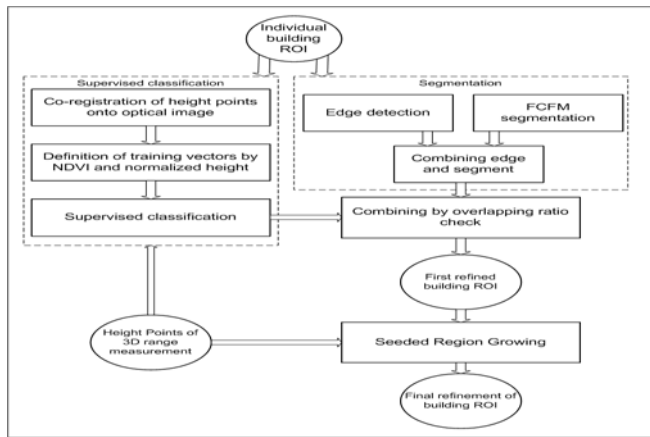


Figure 3. ROI Refinement scheme

$$P(\omega_i) = \frac{m * w}{M} \quad (5)$$

where M = total number of 3D range points in the ROI,
 m = 3D points of some height and NDVI range, which is assumed from the iteration process
 w : weight value from normalized heights

The results of this supervised classification stage are then combined with segments to preserve edges using the FCFM (fuzzy clustering and fuzzy merging) method (Looney 2002).

To begin with, the edge lines within a building ROI are extracted and the remaining parts are pre-segmented. Then, the separated edge portion is combined by a distance measurement in colour space along its path. For 8-way connectivity, the nearby segments are checked and the nearest colour distance is measured to all of the surrounding segments' centres.

$$d_i = \min(\|u_i - c_k\|^2) \quad (6)$$

where C_k : the centre of cluster k ,
 u_i : colour vector of edge points

Now the edge preservation is completed in all the other processing chains. Secondly, FCFM, whose prototype class number depends on the pixels in region P , is applied to a pre-

defined region, P . The relationship between the prototype's class number and pixels can be expressed as follows.

$$C_n = 1 + \log(|S|/500) \quad (7)$$

where $|S|$: the number of pixels from a predefined segment S
The cluster number is adjusted by the internal logic of FCFM once more, so that optimal numbers of segments are produced keeping the edge parts, because relatively noisy portions of segments are already removed as the detected edges. The next step is the data fusion between FCFM colour segmentation and the results of the Bayes classifier. This is performed by measuring an overlap ratio and then reassembling. The overlap measurement between the FCFM segment and the building part by a Bayes classifier is given

$$p(x) = N \left(\frac{|R_{\max}| - |R_{\min}|}{|R_x| - |R_{\min}|} \right) \log(|R_t|/|R_x|) \quad (8)$$

where $|R_t|$: vector number of a region t

$|R_x|$: vector number of a cluster x

$|R_{\max}|$: vector number of maximum size region

$|R_{\min}|$: vector number of minimum size region

N : constants by clusters $N=1$ building, $N=0.7$ tree, $N=0.5$ bare filed

The results are shown in Figure 4. On the opposite side of the direction of the Sun (i.e. shadow side), the edges are clearer. Consequently, the boundaries of those parts show a good agreement with an estimated straight line. However, one problem for this scheme is the hidden part of the building in shadow, where the distances of the colour space are all similar in spite of the difference in the multi-spectral signature, and as the supervised classified scheme doesn't work correctly, the correct building boundaries are not detected.



Figure 4. The first refinement result of building ROI by clustering scheme (missing Lidar points over some “hidden” buildings results in no identification.)

To compensate for the weakness of this method, the SRG (Seeded Region Growing) algorithm developed by Adams and Bischof (1994) was introduced in the last part of the refinement. One difference with the original SRG is the use of multiple seed points, which are matched onto the roof structures by the previous registration work. From clusters of seed points, the building area grows until there is a convergence of pixel number by updating the statistical value of each cluster. The result of the SRG stage is shown in Figure 5.

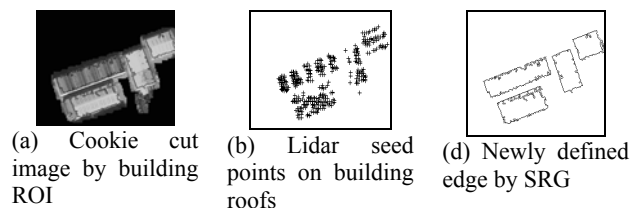


Figure 5. Final building outline examples refinement by SRG

2.3 Identification of target shape

2.3.1 Building

The boundary defined through the SRG is relatively accurate but still contains some undulation. There is a great deal of published methods for the generalization of detected building primitive from multi-spectral images and Lidar. The simplest method is to use the Douglas-Peucker Line Approximation Algorithm (Hershberger and Snoeyink 1992). However, a problem using their scheme is encountered because building shapes are irregular in our test area so that the discrimination between noise and true building edges is very difficult. A simple polygon approximation from Wall and Danielsson (1984) is here applied to the refined building from the SRG and shows satisfactory results

2.3.2 Tree crown identification

The main problem addressed here is the lack of information required for automated individual tree detection (texture, crown boundary) as it is missing in our 1 metre resolution imagery. In our case, Lidar points, even though the resolution is not high enough to precisely model or count individual trees can be applied synergistically with the optical data. The starting point is NDVI, because normalized colour using R-G-B scheme doesn't provide sufficient information for tree detection because of the illumination effect. Also normalized colour transformations are not useful because these are based on the R-G-B colour space analysis. Our own colour scheme uses the following colour spaces:

Ch 1 : (R-G)/(R+G), Ch 2 : (G-NIR)/(R+NIR), Ch 3 : NDVI

This algorithm is only applied to the channels within areas with high NDVI (>0.2) values. The shadowed areas must be removed to avoid classification problems. The definition of a shadow mask is, fortunately, very simple. The pan-sharpened image is transformed using the USGS Munsell HSV scheme and a k-means classification is applied to this image. Using this method, the shadow area can be easily defined and removed in consecutive processing stages. The Lidar points in the high NDVI area can be split into two parts using thresholds of n-DEM height > 6m for points defined as trees and n-DEM height < 0.5m for grassland points. These selected points can then be used to provide training vectors for a maximum likelihood classification. The classification results based on these approaches are in extremely good agreement with trees and grassland. Using tree masks from the classification, the Lidar points from the tree crown areas can be re-collected. Kriging has been established as the most reliable method to keep the continuous change of height value in a round shape. It shows there are relatively clear divisions between DEM peaks. Therefore the key issue is how these DEM peaks can be divided. Wood (1996) studied the detection of topographic features from DEMs. Usually, a sloping surface that is concave in the cross-sectional direction is a channel so the channel points of a tree DEM can be detected using Wood's method. Each tree crown is enclosed by a detected channel point so we can split the tree crown by removing weakly connected components using channel points. In each tree DEM patch, ellipse fitting can be applied using Pilu et al. (1999)'s method. Then the eccentricity is checked. If this value is higher than some threshold, in the weakly connected parts, one more split is made and the ellipse is re-fitted. This process is continued until patches are fitted or have fewer points than a given lower threshold.

3. RESULTS & ASSESSMENTS

The final three products consist of - DTM, boundaries of building structures and ellipses representing tree crowns. These products have been verified using GIS data (OS® MasterMap®) and visual inspection.

3.1 DTM

A DTM covering an area of 8 by 8 km was constructed (Figure 6) in 4 stages using the hierarchical gridding scheme for the entire east London area. A quality assessment comparing commercial DTMs (such as the 50m OS® Panorama®) is impossible because of the large resolution differences but visual inspection in detail shows large landscape objects like the Millennium dome can be successfully removed and small natural alternations in height are well preserved.

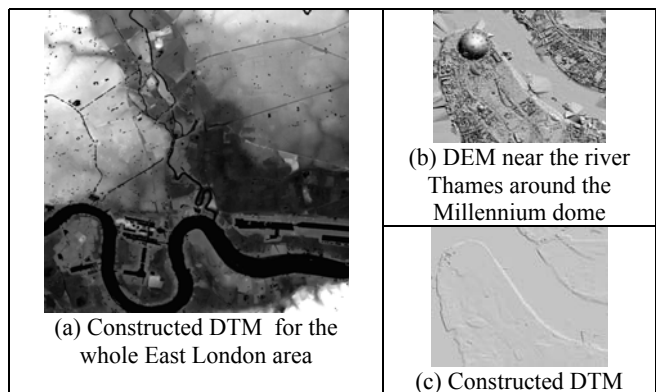


Figure 6. Constructed DTM

3.2 Building boundaries

The Building Detection Metrics (Shufelt & McKeown, 1993) scheme is used here to evaluate the accuracy of building outlines compared with OS® MasterMap® data. In the Shufelt & McKeown scheme, quality assessment factors are defined as below.

$$\text{Building Detection Percentage} = 100 \text{ TP} / (\text{TP} + \text{FN})$$

$$\text{Branching Factor} = \text{FP} / \text{TP}$$

$$\text{Quality Percentage} = 100 \text{ TP} / (\text{TP} + \text{FP} + \text{FN})$$

where TP: True Positive (Both data sets (detected building and OS data) classify the pixel as being part of a building)

TN: True negative (Both data sets classify the pixel as being part of the background)

FP: False Positive (Detected data set classifies the pixel as a building, OS data set classifies it as background)

FN: False Negatives (Detected data set classifies the pixel as background, OS data set classifies it as a building)

Figure 7 (a) and Table 1 shows the detection accuracy of building boundaries in a 1.0 by 1.5 km area using the method described here. As seen in Figure 7 (b), small building structures such as houses and irregular shaped buildings are successfully detected.

Building Detection Percentage	74.97 %
Branching Factor	0.19
Quality Percentage	65.67 %

Table 1. Quality assessment of detected building boundaries cf. Parish et al., (2003)

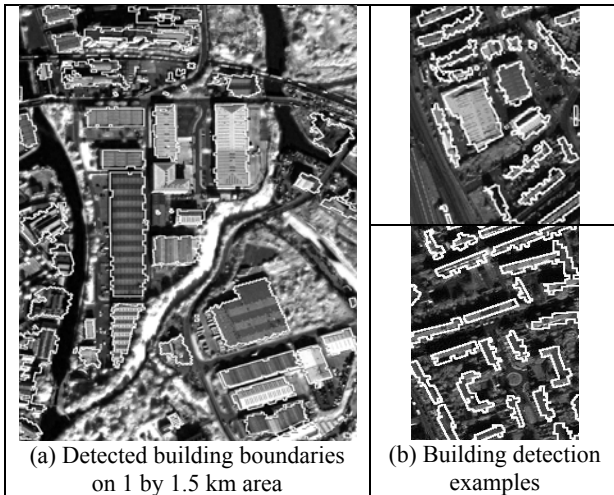


Figure 7. Detected building boundaries

3.3 Tree crown

For the entire 8 by 8 km area, tree crowns were extracted. Some isolated individual tree crowns well match with the optical images (Figure 8 (b)). However, in aggregated tree clusters, it is not so clear whether the fitted crown ellipse is correct or not because both the visual image and the DEM are too low a resolution. Also, overall accuracy including results for forest areas are not so good when comparing locally detected tree crowns in the 1.5 by 1 km sub area (Figure 8 (a)). That's because of the local variation in spectral signature.

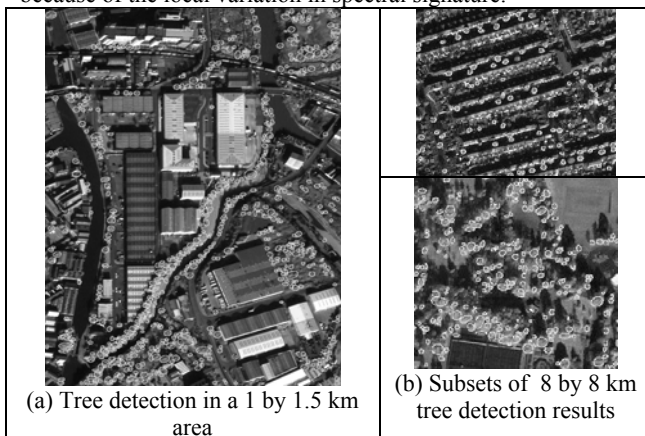


Figure 8. Tree detection in a 1 by 1.5 km area

4. SUBSIDENCE RISK MAPPING

Kelvin (2003) used the tree crown centre locations as detected here together with the OS® MasterMap® digital map data and the surface and sub-surface geology from the BGS DiGMapGB-50 dataset to assess the impact of tree locations on potential building subsidence. Within the UK, most domestic subsidence occurs on shrinkable clay soils. Vegetative desiccation is a prime cause of clay shrinkage. When allied with the aforementioned commercial datasets, the tree location data allows mapping of the desiccation zones. If a simple risk classification is adopted, a relatively straightforward method of identifying potential occurrences of subsidence can be used (Figure 9). This offers significant improvements over existing subsidence risk assessment methodologies, such as those carried out for insurance purposes, which do not fully account for the spatial distribution of the causative factors. This method offers much potential for future refinement. The publication of more detailed studies of vegetative desiccation characteristics would

improve the potential accuracy of the findings, and the possibility exists of adding value to the OS® MasterMap® data in the form of information relating to building age and condition. It is to be hoped that this method will generate results consistent with those of existing techniques, such as PSInSAR. If this is the case, then the techniques developed within this paper would be applicable for predictive purposes within the context of urban development.

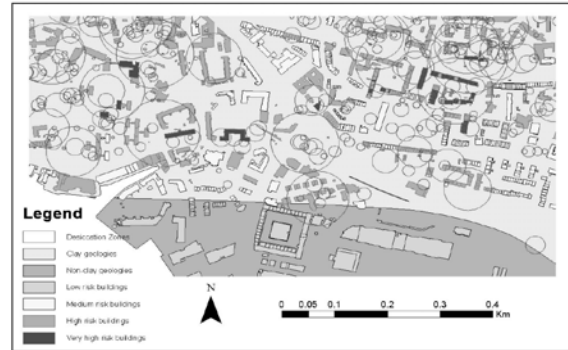


Figure 9. Subsidence Riskmap accounting for buildings influenced by two or more desiccation zones using tree data derived using the methods described here. (taken from Figure 4.11 of Kelvin, 2003). Geology data: IPR/43-39C British Geological Survey. © NERC. MasterMap data: Ordnance Survey ©Crown Copyright.

5. CONCLUSION

A general landscape object detection method for a very large urban areas has been demonstrated here. It consists of focusing by DTM construction, refinement of ROI by data fusion between 3D range data and multi-spectral signature and object identification by boundary generalization and fitting. Assessments of final products – DTM, building and tree crown, shows acceptable quality compared with ground truth like GIS data sets and appears to be reliable under visual inspection considering the limited resolution of the 3D range data. However, object detection quality should be able to be upgraded with the introduction of more reliable machine vision algorithms such as a robust generalization process for building boundaries and splitting methods for tree crown reflectance using the optical image rather than the Lidar DEM.

Domestic subsidence is a well-known problem when buildings with shallow foundations (in the UK much of the housing stock is over 100 years old) lies on clay soils with large amounts of tree cover. Central to this is the ability to determine individual tree locations and their proximity to buildings. Using external information on (a) soil geology; (b) building age; (c) tree root damage potential depending on tree type; (d) tree height (determined from lidar), landscape object detection result in this research can provide a map of buildings under risk from subsidence.

ACKNOWLEDGEMENTS

The authors would like to thank BNSC and Infoterra Ltd for supporting this research under the LINK programme as well as providing the Lidar data-set. We also thank Nicke Coote of the Ordnance Survey for kindly providing the OS® MasterMap® data.

REFERENCES

- Adams, R., L. Bischof, L., 1994, Seeded Region Growing, *IEEE Transaction on Pattern Analysis and Machine Intelligence*, 16(6), pp. 641 – 647.

- Axelsson, P., 1998. Processing of laser scanner data – algorithms and applications. *ISPRS Journal of Photogrammetry & Remote Sensing*, 53(2) pp.138-147.
- Baltsavias, E., Pateraki, M., Zhang, L., 2001. Radiometric and geometric evaluation of Ikonos Geo images and their use for 3D building modelling. *Proceeding of Joint ISPRS Workshop High Resolution Mapping from Space 2001*, Hannover, Germany, 19-21 September.
- Brenner, C., Haala, N., 1999, “Extraction of buildings and trees in urban environments,” *ISPRS Journal of Photogrammetry and Remote Sensing*, 54, pp 130-137.
- Chaudhuri, B.B., Shankar, B.U., 1989, An Efficient Algorithm For Extrema Detection In Digital Images, *Pattern Recognition Letter*, (10), pp. 81-85.
- Fraser, C.S., Hanley, H.B., Yamakawa, T., 2001. Sub-metre geopositioning with Ikonos GEO imagery. *Proceeding of Joint ISPRS Workshop High Resolution Mapping from Space 2001* Hanover, Germany , 19-21 September.
- Grodecki, J., 2001, IKONOS Stereo Feature Extraction—RPC Approach, *Proceedings of ASPRS 2001 Conference*, St. Louis, US, 23-27 April.
- Grodecki, J., G. Dial, 2001, *IKONOS Geometric Accuracy* , *Proceeding. of ISPRS Workshop on High Resolution Mapping from Space 2001* Hanover, Germany ,19-21 September.
- Gong, P., Sheng, Y., Biging, G.S., 2002, 3D Model-Based Tree Measurement from High-Resolution Aerial Imagery, *Photogrammetric Engineering and remote sensing*, 68(11), pp.1203-1212.
- Hershberger, J., Snoeyink, J., 1992, Speeding Up the Douglas-Peucker Line-Simplification Algorithm, *Proceedings of the 5th International Symposium on Spatial Data Handling*
- Kelvin. J. 2003, Exploring the potential for GIS-based subsidence risk assessment. *MSc GIS dissertation, University of London, UK*, p72.
- Lin, C., Nevatia, R., 1998, Building Detection and Description from a Single Intensity Image, *Computer Vision and Image Understanding*, 72(2), pp.101-121.
- Looney, C. G., 2002, Interactive clustering and merging with a new fuzzy expected value, *Pattern Recognition Letter.*, 35, pp. 187–197.
- Maas, H. G., Vosselman, G., 1999, Two algorithms for extracting building models from raw laser altimetry data, *ISPRS Journal of Photogrammetry and Remote Sensing*, 54 (2/3), pp.153-163.
- Kim, T.J., Muller, J.P., 1999, Development of a graph-based approach for building detection, *Image and Vision Computing* 17. pp.3–14.
- Kim, J. R., Muller, J.- P., 2002. 3D reconstruction from very high resolution satellite stereo and its application to object identification. *Symposium on Geospatial theory, Processing and Applications, Ottawa. Joint International Symposium on " Geospatial theory, processing and applications"*, , Ottawa, Canada. 8-12 July
- Kraus, K., Pfeifer, N., 1998, Determination of terrain models in wooded areas with airborne laser scanner data, *ISPRS Journal of Photogrammetry & Remote Sensing* 53 (4), pp.193–203.
- Lohmann, P., Andreas Koch, A., Michael Schaeffer, M., 2000. , Approach to the filtering of laser scanner data *International Archives of Photogrammetry and Remote Sensing* 34 (B3/1), pp.534-541.
- Parish, B., Muller, J-P., Kim, J-R., 2003. Quality assessment of automated building identification in IKONOS imagery. *ISPRS Journal of Photogrammetry & Remote Sensing submitted*
- Pilu, M., Fitzgibbon, A., Fisher, R., 1999, Direct least square fitting of ellipses, *IEEE Transactions on Pattern Analysis and Machine Intelligence* 21 (5), pp.476-480.
- Pollock, 1998. Individual tree crown recognition based on synthetic tree crown image model, In D.A Hill and D.G Leckie (Eds.). *Proceeding of international forum on Automated Interpretation of high spatial resolution Digital Imagery for the forest*. pp.24-34, Victoria, B.C ; Canadian forest service, Pacific forest center
- Roux, M., MacKeown, D.M., 1994, Feature matching for building extraction from multiple view, *Proceedings of ARPA Image understanding Workshop*, pp.331-349.
- Shufelt, J., McKeown, D.M., 1993, Fusion of monocular cues to detect man-made structures in aerial imagery, *Computer Vision and Image Understanding* 57(3) pp.307–330.
- Straub, B., 2003, A Top-Down Operator for the Automatic Extraction of Trees - Concept and Performance Evaluation, *Proceedings of the ISPRS working group III/3 workshop '3-D reconstruction from airborne laserscanner and InSAR data'*, Dresden, Germany, 8-10 October.
- Vosselman, G., 2000. Slope based filtering of laser altimetry data. *International Archives of Photogrammetry and Remote Sensing*, 33(B3/2), pp. 935-942.
- Wall, K., Danielsson, P.E., 1984. A fast sequential method for the polygonal approximation of digitized curves, *Computer Graphics and Image Processing*, 28(3) pp. 220–227.
- Wood, J., 1996, The Geomorphological Characterisation of Digital Elevation Models. *Ph.D thesis, Department of Geography, University of Leicester, Leicester, UK.*
- Zhang, Y, 2001, Texture-Integrated Classification of Urban Treed Areas in High-Resolution Color-Infrared Imagery *Photogrammetric Engineering and remote sensing*, 67(12) pp.1359-1367.